UCRL 8007

UNIVERSITY OF CALIFORNIA

Radiation Laboratory

MASSES AND DECAY PROCESSES OF CHARGED HYPERONS

BERKELEY, CALIFORNIA

DISCLAIMER

UCRL-8007
Physics and Mathematics

UNIVERSITY OF CALIFORNIA
Radiation Laboratory
Berkeley, California

Contract No. W-7405-eng-48

MASSES AND DECAY PROCESSES OF CHARGED HYPERONS

Peter C. Giles

(Thesis)

October 7, 1957

Printed for the U. S. Atomic Energy Commission

MASSES AND DECAY PROCESSES OF CHARGED HYPERONS

Contents

MASSES AND DECAY PROCESSES OF CHARGED HYPERONS

Peter C. Giles

Radiation Laboratory
University of California
Berkeley, California

October 7, 1957

ABSTRACT

The decay in nuclear emulsion of charged hyperons yields information about the hyperon masses and their lifetimes, as well as the K^--meson mass. The masses obtained in this study are

$$M_{\Sigma^+} = 2327.4 \pm 0.6\ m_e,$$

$$M_{\Sigma^-} = 2340.3 \pm 1.4\ m_e,$$

$$M_{K^-} = 965.1 \pm 1.2\ m_e.$$

The best lifetimes are

$$\tau_{\Sigma^+} = 0.87\ ^{+\ 0.13}_{-\ 0.10} \times 10^{-10}\ \text{sec},$$

$$\tau_{\Sigma^-} = 1.7\ ^{+\ 1.2}_{-\ 0.5} \times 10^{-10}\ \text{sec}.$$

Furthermore, no evidence is found for a forward-backward asymmetry or anisotropy in the decay process.

INTRODUCTION

In recent years several new particles have been discovered in studies of cosmic radiation. In particular, charged particles of trans-nucleonic mass were first noticed by Leighton,[1] using a cloud chamber detector, and by Levi-Setti,[2] using photographic emulsion as detector. Present nomenclature denotes these particles Σ^+ and Σ^- hyperons. Examination of their properties was limited by the rarity with which these hyperons are observed in cosmic radiation. However, in 1955 Hornbostel and Salant[3] observed charged hyperons emitted from K^--meson interactions with photographic emulsion nuclei. Such a reaction is consistent with the Gell-Mann strangeness scheme.[4] The hyperons and the K^- mesons all have the same strangeness, $S = -1$, hence no change in strangeness occurs in the reaction. If there is no change in "S", a fast interaction such as this may proceed.

Since the time of the observation by Hornbostel and Salant considerable effort has been made to study hyperons emitted from K^- interactions. Notable among these are the hydrogen bubble chamber program to study K^- interactions with hydrogen,[5] and several nuclear emulsion programs studying the interactions of K^- mesons with emulsion nuclei.[6-10] Negative K^--meson "beams" have been created both at the Brookhaven Cosmotron and at the Berkeley Bevatron. In 1956 a low-momentum separated K^- beam was developed at the Bevatron wherein π^- mesons are virtually eliminated.[7] π^- mesons, because of their strong interactions with nuclei, are the main source of background; their flux density dictates the limit of exposure. Elimination of π^- mesons has allowed us to accumulate more K^- mesons, by orders of magnitude, in a nuclear emulsion stack than was previously possible. In turn, sufficient charged hyperons are produced in the emulsion to allow more extensive analysis than ever before possible.

Several measurements made on the properties of charged hyperons are described in this paper. The mass of the Σ^+ hyperon is measured with improved statistical accuracy. Additional information about the masses of the K^- meson and the Σ^- hyperon are included.

The Σ^+-lifetime measurement is much improved over previous emulsion measurements, and an estimate is made of the Σ^--hyperon lifetime. The angular distribution of the hyperon decay products is given. These data bear on the spin and parity-conserving characteristics of hyperons. All the above information is based directly on measurements made of the hyperon decay process. In addition, the masses of the K^- meson and of the Σ^- hyperon require data from measurements made on the interactions of K^- mesons with free protons. These are present as hydrogen nuclei in the emulsion.

EXPERIMENTAL APPARATUS

The K^--meson beam is created by the full-energy proton beam in the Bevatron: 6.2-Bev protons strike a 0.5-by-1-by-3.5-inch copper target block. This target is affixed to a flip-up device and is located at the 73^o position near the north tangent tank in the Bevatron. Negatively charged particles are emitted in the forward direction with respect to the primary proton beam, and are deflected by the Bevatron magnetic field so as to pass between two magnet yokes. The rather narrow yoke separation serves as a collimator and momentum analyzer. The negatively charged particles proceed through this separation and pass out radially. Figure 1 represents schematically the physical arrangement. At the exit point of the Bevatron shroud the particles have a central momentum of 427 Mev/c, and an intensity of 6×10^3 particles/cm^2/10^{10} protons on the target. The π^-/K^- ratio is 3000/1. The beam then passes through a quadrupole focusing magnet. From there it is decelerated in a polyethylene degrader placed at the entrance to the analyzing magnet. The nominal thickness of the degrader is 19.4 g/cm^2. After the pion has traversed the degrader its momentum is reduced to 394 Mev/c, and the K^- momentum to 300 Mev/c. The analyzing magnet then effects a spatial separation upon the two momentum groups. K^- mesons are deflected nearly 180^o.

The final separation between the peaks of the K^- and π^- beams is about 19 inches. The detector was a stack of 240 9-by-12-inch nuclear emulsion pellicles. The average pellicle thickness before processing was about 640 microns; the over-all stack height was 6 inches. The stack was positioned during exposure with the pellicles oriented horizontally. The K^- beam enters the 12-by-6-inch face, parallel to the pellicles. This stack is denoted 2B. In addition, a smaller test stack consisting of 120 3-by-6-inch pellicles is used as a source of data. It is denoted 1U. The 1U stack was oriented similarly to the 2B stack during exposure, with the K^- beam entering the side, normal to the 6-inch length and 3-inch height. The K^- flux at the stack position is 50 K^-/cm^2/10^{13} protons on the target. The momentum

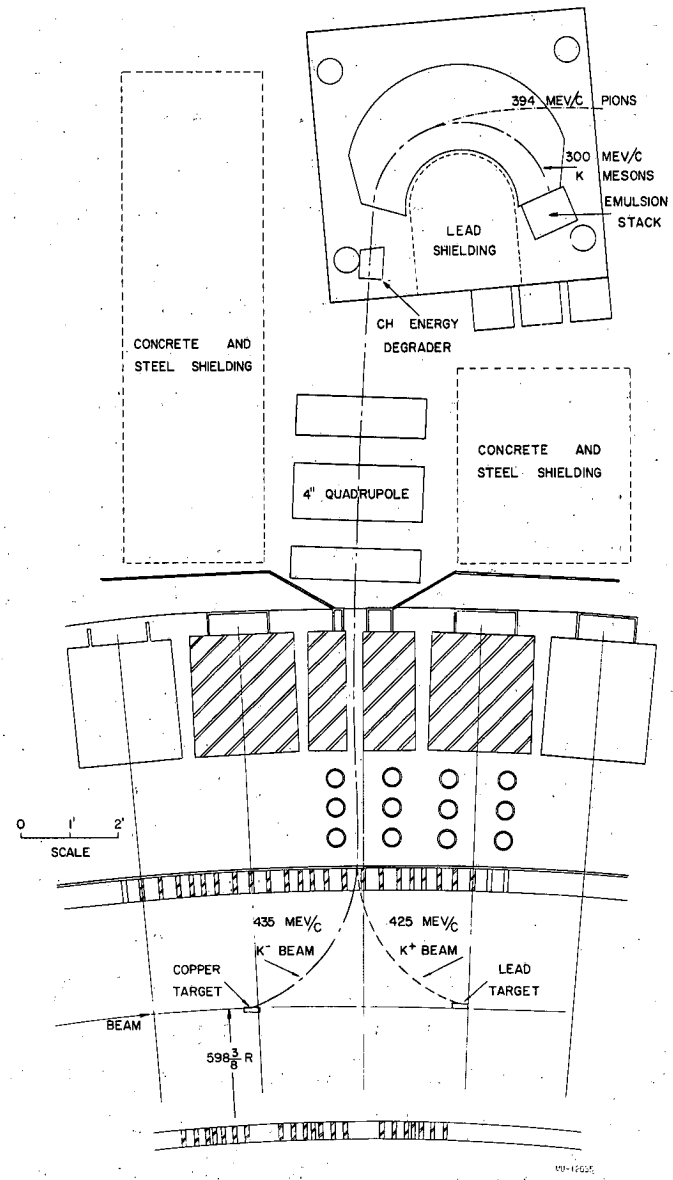

Fig. 1. Experimental arrangement of the separated K^- beam. Negative particles (π^- and K^-) leave the copper target, are deflected by the Bevatron magnetic field, and pass through the iron magnet yoke. They travel on through the quadrupole focusing magnet and are decelerated in the polyethylene degrader. π^- mesons and K^- mesons follow the paths through the analyzing magnet as indicated.

gradient here is 1.6 Mev/c per cm, with a ± 2% dispersion in momentum. The location of the K^- peak is uncritical; the stack received nearly uniform exposure azimuthally. The background constituents of the "separated K^- beam" are: μ mesons, 80%; electrons, 10%; and π mesons, 10%. The ratio of minimum-ionizing tracks to K^- tracks is 800/1. Mu mesons occur as the result of π-meson decay in flight along the channel from target to detector. Because they are weakly interacting, the μ-meson flux does not hinder scanning. It is estimated that more than 95% of all particles that are twice minimum ionization and that enter within 10^o of the expected beam direction are K^- mesons.

TECHNIQUE

Hyperon Identification

When K^- mesons interact with emulsion nuclei, a charged hyperon occasionally is seen as a reaction product. The scanning procedure for finding charged hyperons is as follows: Tracks of twice minimum ionization are picked up in the microscope 1 millimeter from the entrance edge of the pellicle. An experienced scanner is about 95% efficient in picking genuine K^- mesons. They are then followed until they either decay or interact with the emulsion nuclei. Interactions are classified according to the number of secondary prongs: zero-, one-, two-, or many-pronged stars. Naturally, charged hyperons are emitted only from the latter three categories of interactions. The prongs from one- and two-pronged stars are followed to their ends, and examined for the existence of a decay particle. The prong may or may not decay in flight. Those secondaries coming from larger stars are followed either to the surface of the pellicle in which they are created or to their ends if they stop or decay in that pellicle. These prongs, also, are examined for decay particles.

A charged hyperon is identified in a number of ways. The Σ^+ hyperon may be positively identified as a particle with protonlike appearance which decays at rest into either an approximately 19-Mev proton or a 90-Mev pion. It also may be identified if it decays in flight into a proton. Such decays in flight usually have an obvious change in ionization or multiple scattering from primary to secondary. There is also a strict relation between the range of the decay proton, its angle of emission in the laboratory system, and the velocity of the hyperon at decay. By use of these criteria, ambiguous proton-scattering events may be eliminated. The Σ^- hyperon may be positively identified as a proton-simulating particle which interacts at rest, forming a small star. These appear somewhat more energetic than μ-meson stars. Many Σ^- hyperons come to rest and form no apparant star. Of these, some are identifiable by an associated Auger electron. Either a Σ^+ or Σ^- hyperon may decay in flight into a charged pion and a neutron.

They are easily identified as hyperons; their charge may be ascertained only by following the pion secondary. Examples of Σ^+ decaying at rest into a proton, Σ^+ decaying into a charged pion, and Σ^- interacting at rest are represented in Fig. 2.

Hyperon Reactions

Three elementary reactions involving charged hyperons lead in an obvious way to the measurement of the masses of the K^- meson and the two charged hyperons:

(a) The decay at rest of the Σ^+ hyperon. Information about its mass is most readily obtained from the decay process, $\Sigma^+ \rightarrow p + \pi^0$, at rest in emulsion. A measurement of the proton range describes the proton energy and momentum through the known range-energy relation for nuclear emulsion. The Q value of the above reaction measures directly the mass of the Σ^+ hyperon.

(b) The interaction at rest of the K^- meson with hydrogen nuclei, $K^- + p \rightarrow \Sigma^+ + \pi^-$, at rest. Hydrogen is a constituent of the gelatin and of the water absorbed in the emulsion. As described above, the Σ^+ range gives a measure of its energy. The Q value of this reaction relates the K^- mass to the Σ^+ mass.

(c) The same interaction as (b) but with the oppositely charged products: $K^- + p \rightarrow \Sigma^- + \pi^+$, at rest. The difference in Q values of Reactions (b) and (c) clearly measures the difference in mass of the Σ^+ and Σ^- hyperons. The mass difference is independent of the K^- mass, and of uncertainties in the range-energy relation for nuclear emulsion.

The most useful information contained in each reaction above is manifested in the range of the heavy secondary particle. The credibility of the final mass values depends then upon the accuracy of the range measurements and of the range-energy relation.

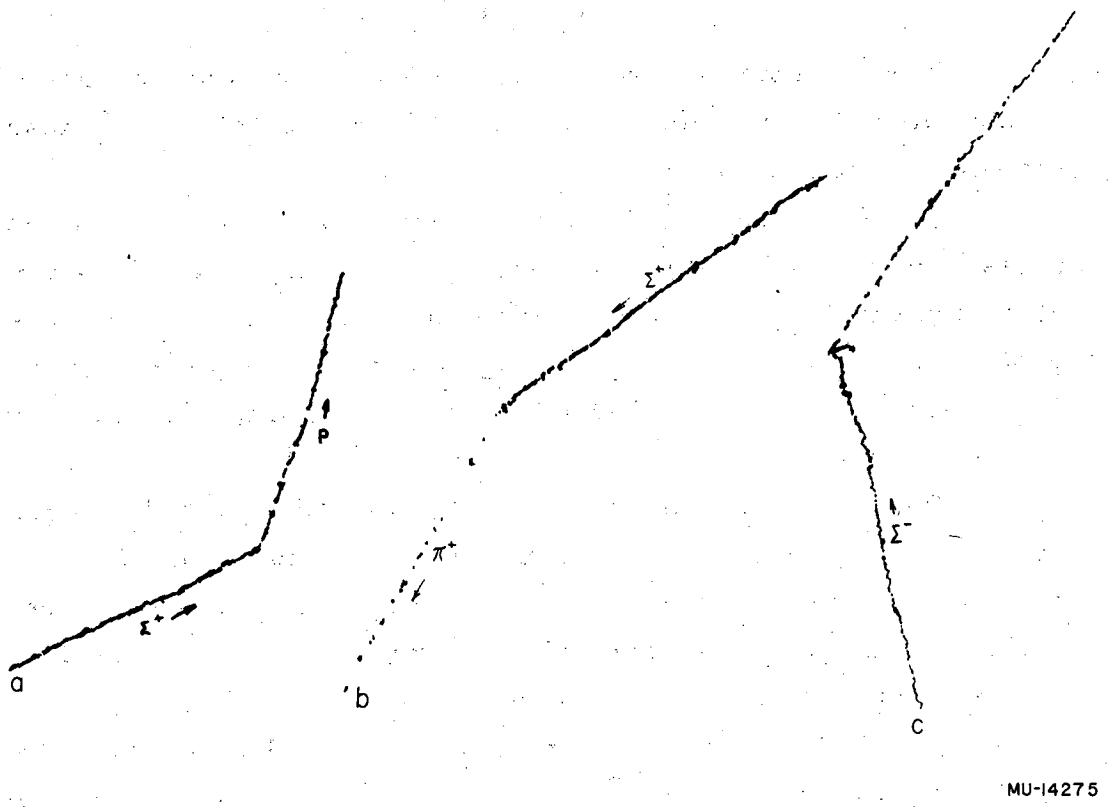

Fig. 2. Tracings of tracks in emulsion. A. The decay at rest of a Σ^+ hyperon. It decays into a neutral pion and the proton that is seen leaving the hyperon ending. B. Another Σ^+ hyperon decaying at rest, this time into a neutron and the minimum-ionizing π^+ meson. C. A hyperon interacting at rest with an emulsion nucleus.

Range Measurements

The range of a charged particle penetrating nuclear emulsion is measured with reference to the microscope coordinate system. The Z axis is defined as the optic axis of the microscope. The X and Y axes lie in the plane of the microscope stage and form a mutually orthogonal coordinate system with the Z axis. Owing to the scattering of particles as they pass through matter, the tracks must often be treated as a number of relatively straight segments. The projected lengths of each segment on the X and Y axes are measured with stage verniers. The projected length on the Z axis is measured with the fine focus of the microscope. However, nuclear emulsion shrinks in thickness by a factor of more than two during the developing process. Of course this shrinkage affects the Z-projection readings. In order to measure the true laboratory path length at the time of the reaction, the shrinkage factor must be known as accurately as possible. It is discussed in the following section.

Emulsion Density and the Shrinkage Factor

In principle, the shrinkage factor is established by merely measuring each pellicle thickness before and after processing. Under darkroom conditions, however, such direct measurements are unreliable and a less direct approach must be utilized. We use the following procedure: Before disassembling the stack and before processing, we measure the total mass of the emulsion and its total thickness. The thickness measurement most certainly includes some dead space between pellicles. Then, while disassembling the stack, we cut small samples of emulsion in uncritical areas from several pellicles. The densities of these samples are determined by Archimedes' Principle, using carbon tetrachloride of known density. If a stack consists of more than one manufacturer's batch, care is taken that samples are cut from all batches. After the stack is processed, the area of each pellicle is measured. The thickness of each pellicle is measured with the microscope. The mean thickness before processing

is deduced from the pellicle areas, the unprocessed mass of the stack, and the unprocessed emulsion density. The shrinkage factor is simply defined as the ratio of unprocessed to processed mean thicknesses.

After processing, the thicknesses of the pellicles are measured all at one time. The fractional error in the total thickness is very small. However, their thicknesses vary from day to day with the ambient humidity. Therefore it is necessary to measure the pellicle thickness again at the time that a range measurement is made in that pellicle. It is estimated that the "ambient" shrinkage factor is known to 1% in the 2B stack. Because it was necessary to resoak the 1U stack in order to preserve it, the 1U shrinkage uncertainty is estimated as 1.5%.

Naturally the rate of energy loss of a charged particle depends upon the density of the emulsion. The relation is not a linear one, however, for emulsion density varies principally with its absorption of water. The stopping power of water is quite different from that of emulsion, which contains about 75% silver bromide by weight. Figure 3 shows the variation of proton range with emulsion density, as quoted by W. H. Barkas.[11] The range-energy relation is established for emulsion of normal density, defined as 3.815 g/cm^3. All ranges must be corrected for any deviation of emulsion density from this value. For the particles being considered, and with the emulsion densities involved, the correction amounts to less than two microns. The table below lists the densities of the various manufacturers' batches. Stack 2B was composed of six manufacturers' batches, each of slightly varying density.

Emulsion batch	Density (g/cm^3)
1 U stack	3.810 ± 0.003
2 B stack	
Z 9804	3.821 ± 0.003
Z 9806	3.814
Z 9808	3.816
Z 9809	3.830
Z 9810	3.803
Z 9811	3.807

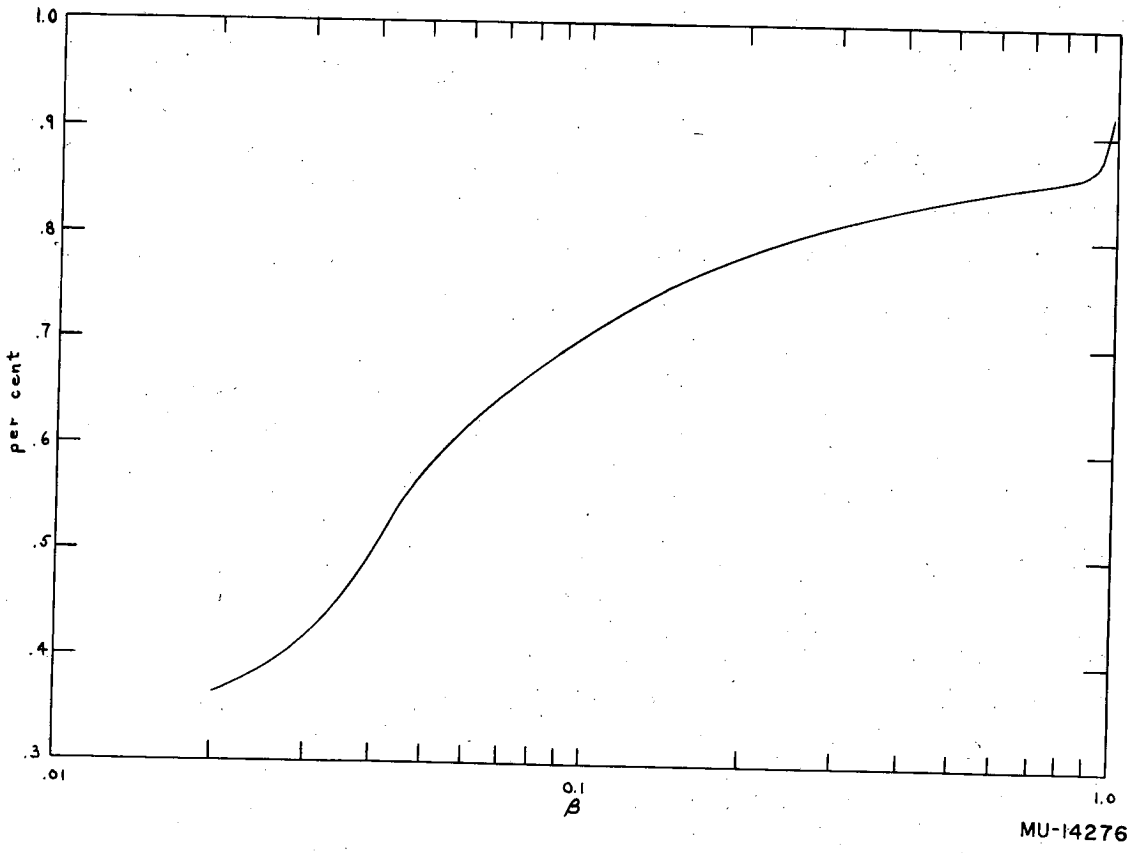

Fig. 3. Variation of proton range with emulsion density. The percent decrease in range per percent increase of emulsion density over the standard density is plotted against the β of the particle.

MASS CALCULATIONS

The Σ^+ Mass

The decay process $\Sigma^+ \rightarrow p + \pi^0$ at rest is the physical process by which the Σ^+ mass may be calculated. The analytic relation

$$M_{\Sigma^+} = (M_p^2 + P_p^2)^{1/2} + (M_{\pi^0}^2 + P_p^2)^{1/2} \qquad (1)$$

expresses the Σ^+ mass in terms of the proton mass, the neutral meson mass, and the proton momentum. The laboratory and center-of-mass systems are identical for events decaying at rest. The mean normalized proton range is the quantity to be considered for determining the proton momentum. The mean range is calculated by weighing the individual ranges according to their uncertainties:

$$\langle R \rangle = \left(\sum_{i=1}^{n} \frac{R_i}{(\Delta R_i)^2} \right) \Bigg/ \left(\sum_{i=1}^{n} \frac{1}{(\Delta R_i)^2} \right), \qquad (2)$$

where $\langle R \rangle$ is the mean weighted range,

R_i is the ith range,

and ΔR_i is the uncertainty in the ith range.

The independent uncertainties ΔR_i have three main sources:

(a) Bohr range straggling,

(b) measurement error,

(c) shrinkage-factor error.

The Bohr range straggling amounts to 1.4% for the ranges involved here. In some cases (very steep tracks) the shrinkage-factor error may be as high as 1%. It depends of course upon the dip angle. The expression for the fractional uncertainty in range from shrinkage error is

$$\frac{\Delta R_{sf}}{R} = \sin^2\delta \; \frac{\Delta S}{S}, \qquad (3)$$

where δ is the dip angle, measured from the azimuthal plane, and $\Delta S/S$ is the fractional uncertainty in shrinkage factor.

The measurement error was set, somewhat arbitrarily, at 1.5 microns per pellicle passed through. Microscope-reading error is the principal contributor to this value. A lesser contributor is the fact that the entrance or exit point of a track in a pellicle can not be defined to better than about one-half micron, owing to the finite size and separation of the silver halide grains. As little uncertainty as this is possible only because the tracks whose range I am considering are all heavily ionizing. In Fig. 4 the normalized proton ranges of 31 Σ^+-hyperon decays are plotted versus $\sin\delta$. It is seen that these ranges are sufficiently independent of δ so as to indicate no appreciable systematic uncertainities in the shrinkage factor. The normalized range distribution is shown in Fig. 5. The mean range is 1674.2 microns; the internal estimate of the uncertainty is ± 4.5 microns. The spread of the distribution is 1.65%. This is somewhat greater than the 1.4% Bohr range straggling, because of the additional uncertainties in measurement and shrinkage factor. The external estimate of the uncertainty is ± 5.0 microns. Using now the Barkas 1957 range-energy relation for standard emulsion,[12] one finds that the above mean range corresponds to the range of an 18.83-Mev proton. There is a statistical uncertainty of 0.3% in the range; in addition there is a systematic uncertainty of 0.5% in this region of the range-energy relation. Because the energy varies with range according to a power law whose exponent is approximately 0.57, the combined uncertainty in the energy is only 0.33%, or 0.063 Mev. The mass of the proton is taken to be 938.23 Mev; that of the neutral pion is assumed to be 135.03 Mev (or 264.3 ± 0.3 M_e). The quantities pertinent to the mass calculation are:

$$M_{\Sigma^+} = (M_p^2 + P_p^2)^{1/2} + (M_{\pi^0}^2 + P_p^2)^{1/2} \qquad (1)$$

$$M_p = 938.23 \pm 0.02 \text{ Mev}$$

$$M_{\pi^0} = 135.03 \pm 0.15 \text{ Mev}$$

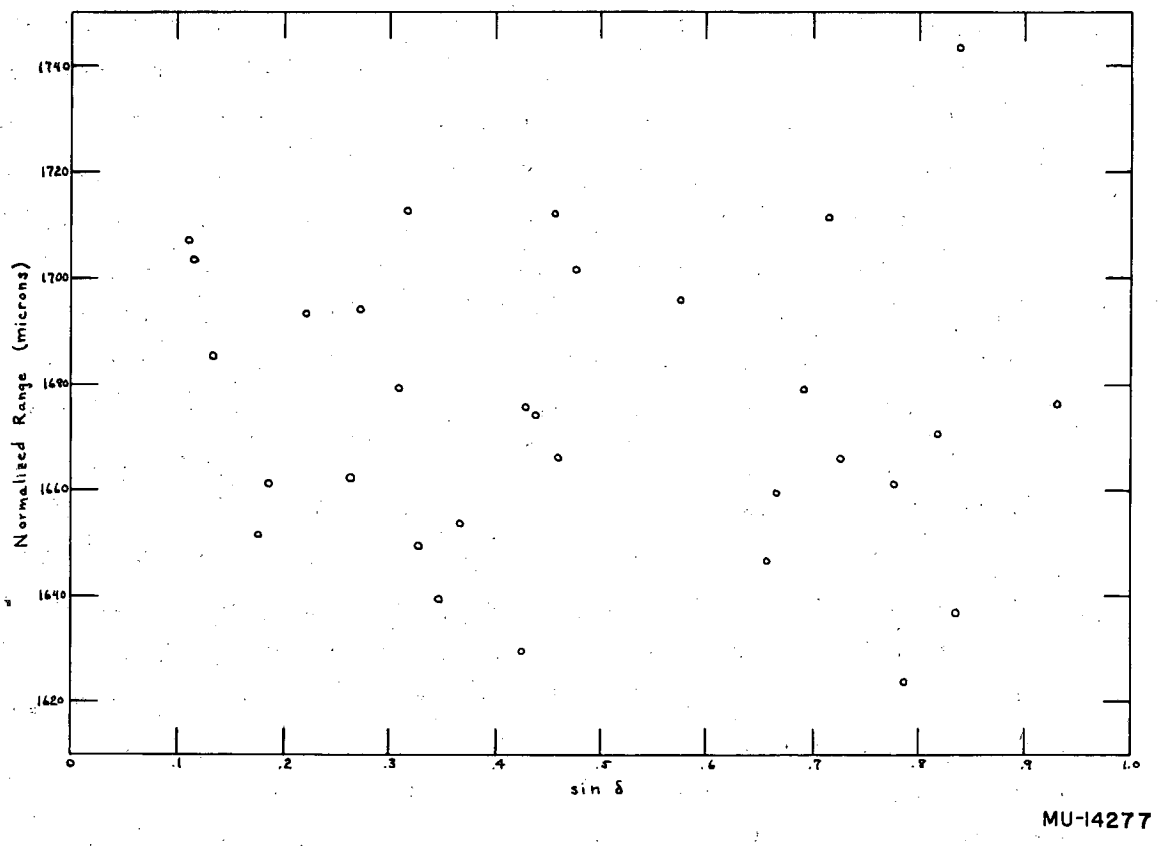

Fig. 4. The normalized ranges of 31 protons emitted by Σ^+ hyperons decaying at rest plotted against the sine of their dip angle at emission.

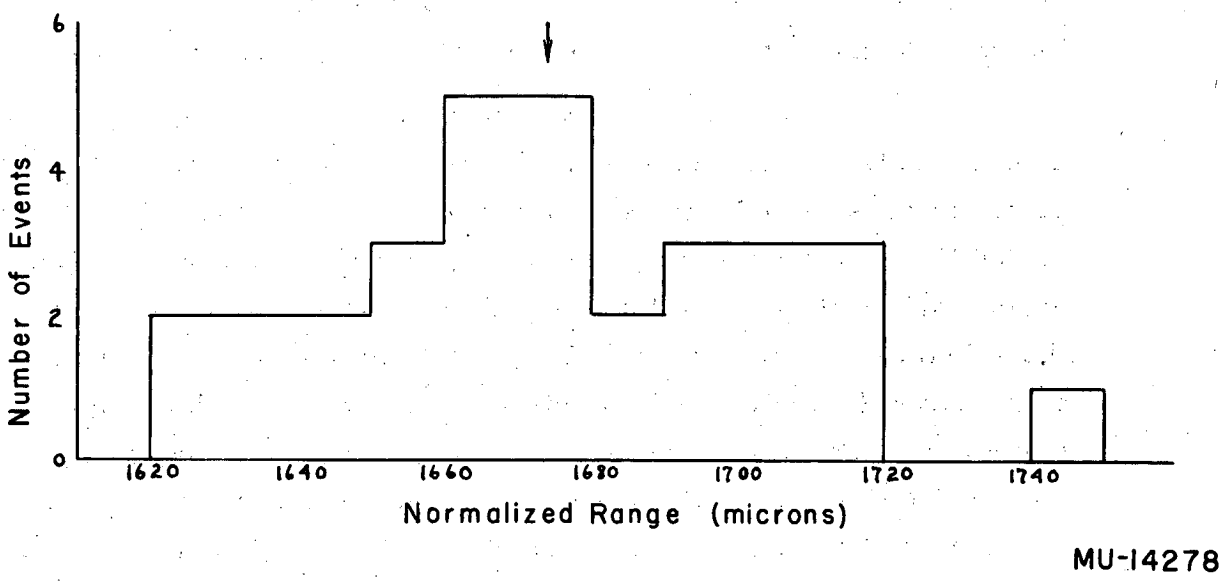

Fig. 5. The normalized range distribution of the same 31 protons as in Fig. 4. The arrow indicates the weighted mean.

Proton range = 1674.2 ± 5.0 microns
Proton energy = 18.83 ± 0.063 Mev
Proton momentum = 188.92 ± 0.31 Mev /c
Reaction Q value = 116.02 ± 0.32 Mev
The Σ^+ mass = 1189.28 ± 0.32 Mev
or 2327.42 ± 0.63 M_e .

Previous estimates of the Σ^+-hyperon mass, all by similar techniques, are 2329.5 ± 1.0 m_e by Gilbert et al.[13] and 2327.4 ± 1.0 m_e by Fry et al.[14]

It should be noted that in principle there is an equal amount of information about the mass from the alternate decay mode,

$$\Sigma^+ \rightarrow \pi^+ + n \text{ at rest in emulsion.}$$

These events are not used for two reasons: (a) Analysis of these events requires considerably more effort for the same information obtained. In the 2B stack slow-electron and single-grain background make it exceedingly difficult to follow the minimum-ionizing pion tracks. In the 1U stack the pion range is large compared with the height and width of the stack (1.5 cm). It is most likely that pions of this range will leave the stack before coming to rest. (b) The uncertainty in the mass from statistical origins is already less than the systematic uncertainty inherent in the range-energy relation. Little statistical improvement could be made by utilizing these events.

The K^- Mass

The interaction at rest of K^- mesons with free protons is the reaction from which information relating the K^--meson mass and the Σ^+-hyperon mass is obtained. The K^- mass is expressed analytically by

$$M_{K^-} = (M_{\Sigma^+}^2 + P_{\Sigma^+}^2)^{1/2} + (M_{\pi^-}^2 + P_{\Sigma^+}^2)^{1/2} - M_p , \qquad (4)$$

where M_{Σ^+} is the Σ^+ hyperon mass, M_p the proton mass, M_{π^-} the charged-pion mass, and P_{Σ^+} the hyperon momentum. As in the procedure outlined in the previous section, the Σ^+ momentum is

measured by its mean range. These ranges are likewise weighted according to their uncertainties. The Bohr range straggling is 1.67% for hyperons of their velocity. The shrinkage-factor errors are again as high as 1%, depending upon the dip angles. The measurement error is again assumed to 1.5 microns per pellicle passed through. The pertinent calculations are

$$M_K^- = (M_{\Sigma^+}^2 + P_{\Sigma^+}^2)^{1/2} + (M_{\pi^-}^2 + P_{\Sigma^+}^2)^{1/2} - M_p$$

$M_p = 938.23 \pm 0.02$ Mev

$M_{\Sigma^+} = 1189.28 \pm 0.32$ Mev

$M_{\pi^-} = 139.63 \pm 0.06$ Mev

hyperon range = 811.7 ± 8.3 microns

hyperon energy = 13.67 ± 0.08 Mev

hyperon momentum = 180.80 ± 0.53 Mev/c

reaction Q value = 102.48 ± 0.51 Mev

the K^- Mass = 493.2 ± 0.6 Mev

or $965.1\ M_e \pm 1.2\ M_e$.

The range-energy uncertainty is neglected. It is small in comparison with the above errors. The above mass value is barely consistent with the K^+-meson mass value of $966.7\ M_e \pm 0.5\ M_e$. Previous K^--mass measurements are $966.2 \pm 1.4\ m_e$ by Fry et al.,[14] and $966.1 \pm 1.6\ m_e$ by Chupp et al.[15]

The Σ^- Mass

By inspection of the reactions

$$K^- + p \rightarrow \Sigma^{\pm} + \pi^{\mp}$$

at rest in emulsion it may be seen that any mass difference between the Σ^+ and Σ^- hyperons will be observed as a $\Sigma^+ - \Sigma^-$ range difference. The difference in kinetic energies of the Σ^+ and Σ^- hyperons is independent of the K^- mass. Their range difference will be nearly independent

of the K^- mass, as well as the range-difference uncertainty. Also, the range-difference uncertainty is nearly independent of the uncertainty in the range-energy relation in this velocity region.

That a mass difference exists was first noted in bubble chamber experiments by Steinberger[16] and first noted in emulsion by Goldhaber.[17] We have three cases of a Σ^+ arising from this reaction, and four of a Σ^-. The average ranges of the Σ^+ hyperon and of the Σ^- hyperon are calculated as before. The sources of error and their magnitudes are of course identical to those listed in the section on K^--meson mass. Figure 6 displays the hyperon mass difference versus the range difference for the above reactions. The calculations necessary for the mass-difference determination are:

Σ^+ mean range = 811.7 ± 8.3 microns

Σ^- mean range = 698.6 ± 6.3 microns

range difference = 113.1 ± 10.4 microns

energy difference = 6.56 ± 0.66 Mev

Σ^+ mass = 1189.28 ± 0.32 Mev

Σ^- mass = 1195.84 ± 0.74 Mev

or 2340.3 ± 1.4 M_e

Some previous calculations assume the equivalence of the K^+ and K^- masses, and use the K^+ meson mass in determining the Σ^- hyperon mass. The above calculation does not make such an assumption. It is independent of the K^- mass. Other estimates of the Σ^- mass are 2341.5 ± 1.5 m_e by Fry et al.,[14] 2342.4 ± 1.7 m_e by Gilbert et al.,[13] and 2340.7 ± 1.3 m_e by Freden et al.[18]

In addition to the interactions of K^- mesons at rest with free protons we have four such interactions in flight. These interactions are not used in the mass measurements, because of the dependence of the calculations on the K^--meson momentum. For events at rest the momentum is exactly zero; in flight, the momentum depends upon angle and range measurements and is subject to their uncertainties. It was found that these events contribute little information to the mass calculations.

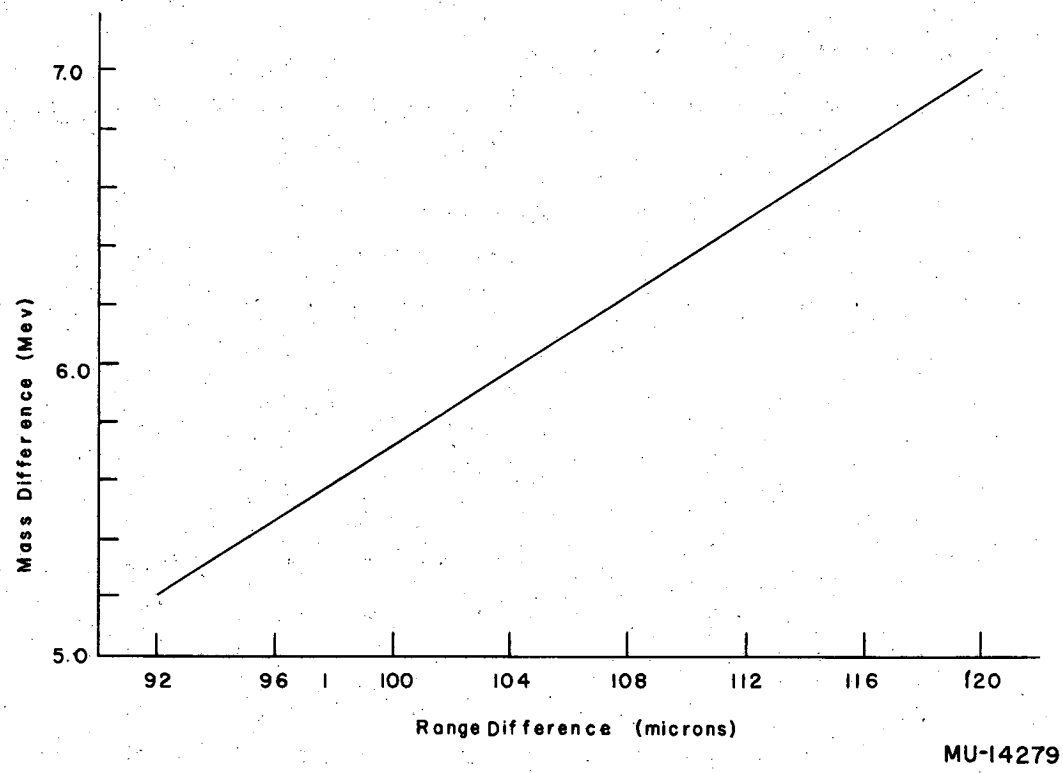

Fig. 6. The Σ^- - Σ^+ hyperon mass difference (in Mev) plotted against the range difference (in microns.) To a first-order approximation, the range difference is independent of the K^- mass.

THE HYPERON DECAY RATES

It is observed that an appreciable fraction of the charged hyperons produced in emulsion decay before coming to rest. Hence the mean life is of the order of magnitude of the moderation time, and measurements of the flight times and of the potential moderation times should yield an estimate of that mean life. The procedure I have used for determining the decay rate is the maximum-likelihood method presented by Bartlett.[19]

The Σ^+-Hyperon Decay Rate Determined By the Proton-Decay Mode

The only straightforward case is that of the proton decay mode of the Σ^+ hyperon. In this case all events are observed and recognized, whether they decay at rest or in flight. According to Bartlett, then, the relative probability P that r represents the true decay rate is given by

$$P = \prod_{i=1}^{F} r e^{-rt_i} \prod_{j=1}^{R} e^{-rT_j}, \qquad (5)$$

where the first product runs over the decays in flight, and the second runs over those at rest. The t_i are the observed flight times, and the T_j are the moderation times. In the two stacks from which the data come, there are 32 decays at rest and 27 decays in flight. The moderation times of those decaying at rest are easily obtained from the hyperon ranges by use of the Barkas tables.[12] The flight time of a hyperon decaying in flight is simply the difference between the initial potential moderation time and the potential moderation time at decay. These times are in turn derived from their corresponding potential ranges. For those hyperons decaying in flight, the residual hyperon range at decay is known quite accurately from the angle of emission and the energy of emission of the decay proton. The initial potential range is the sum of this range and the observed track length up to the decay. The relative probability P defined in the above equation is plotted in Fig. 7. The maximum ordinate represents the

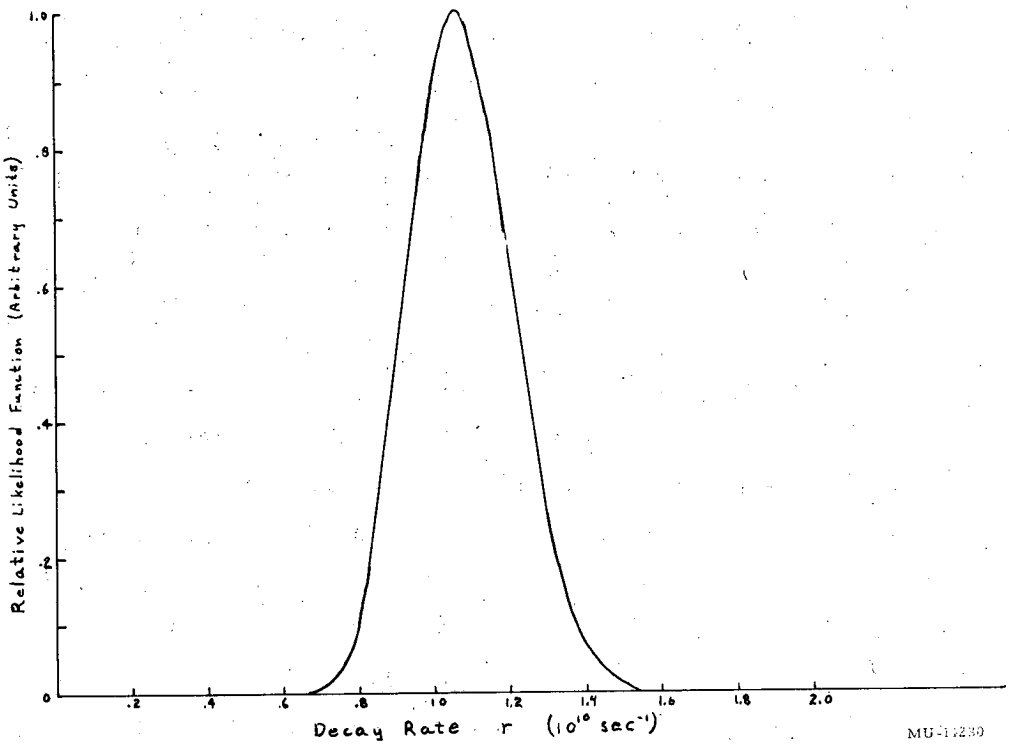

Fig. 7. The relative-likelihood function plotted versus r, the decay rate, for all Σ^+ hyperons decaying through the proton mode. The ordinate is arbitrary.

most likely decay rate of the Σ^+ hyperon, as defined by the proton decay mode. Its value is

$$r_{max} = 1.06 \pm 0.16 \times 10^{10} \text{ sec}^{-1},$$

corresponding to a mean life

$$\tau = 0.94^{+0.17}_{-0.12} \times 10^{-10} \text{ sec.}$$

The limits are for the half-maximum values, and are the statistical uncertainties. Errors in the range measurements are small and generate uncertainties in the most likely decay rate of about 1%, much less than the statistical uncertainties quoted above. The hydrogen-bubble-chamber estimate of the Σ^+ hyperon lifetime is $0.70 \pm 0.10 \times 10^{-10}$ sec (Alvarez et al.,[5]). Other emulsion estimates, based on the proton decay mode, are $0.98^{+0.37}_{-0.21} \times 10^{-10}$ sec by Snow et al.,[20] and $1.38^{+1.39}_{-0.63} \times 10^{-10}$ sec by Seeman et al.[21]

The Hyperon Decay Rate Determined By the Pion Decay Mode

The decay of charged hyperons into charged pions is considerably less easy to analyze than is the proton decay mode. Here both charges contribute to the group, and because of the long pion range the charge cannot be ascertained. There is strong evidence that the hyperon decay rate varies with charge.[5] One approach is to consider only the decays in flight, regardless of charge, and try to calculate some mean decay rate. For such a population the Bartlett expression for the relative probability is

$$P = \prod_{i=1}^{N} \frac{re^{-rt_i}}{1-e^{-rT_i}}, \qquad (6)$$

where r is the decay rate,

t_i is the ith observed flight time,

T_i is the ith initial moderation time.

The measurements of t_i and T_i differ from those measurements of the proton decay mode. The range of the decay proton and its angle of

emission with respect to the hyperon were sufficient information to determine the hyperon energy at decay, and hence the residual potential time. Because the pion range is too great to be followed, this method is useless. Instead, the fractional transmission of the hyperon track at the decay is used to estimate the kinetic energy of the hyperon at decay.

Track Transmission Measurements

The fractional track transmission is defined as the fractional portion of track that is not occupied by developed silver halide grains. It is a function of only the velocity and charge of the particle penetrating the emulsion, and hence in principle can be used to determine the residual range of the particle at the point of measurement. The fractional transmission of a sample hyperon is measured at its decay point and compared with a standard transmission-range calibration curve. In this way the residual range as well as the potential moderation time of hyperons at the point of decay may be estimated. The calibration curve is made by measuring the fractional transmission by tracks of several "flat" stopping protons (i.e., those whose tracks are essentially parallel to the plane of the microscope stage) as a function of residual range, and correcting for the mass difference between protons and hyperons. It is shown in Fig. 8. The fractional track transmission estimate of residual range is much less reliable than a direct range measurement, however, especially where the length of track available for measurement is small, because the residual range varies strongly with the fractional track transmission, as seen in Fig. 8, and because the observed fractional track transmission is a function of the dip angle of the track.

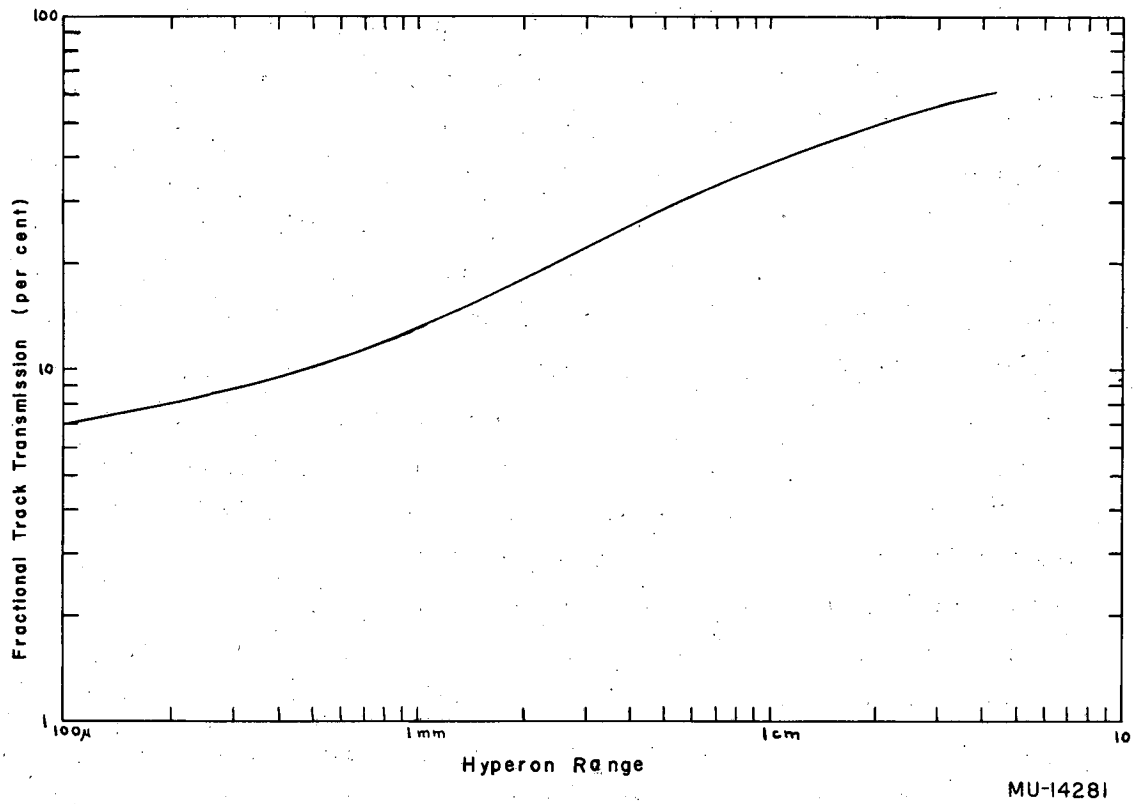

Fig. 8. The fractional track transmission plotted against the hyperon residual range.

Dip-Angle Correction

A simple model of track grains is shown in profile in Fig. 9. The absolute separation is L. The observed separation is

$$L' = (L + 2a) \cos \delta - 2a ;$$

the gap distribution is exponential,[22] i.e.,

$$N(L) \sim e^{-L/L_0} ,$$

where L_0 is a function of the particle velocity. For a particular velocity, a flat track has a mean gap length

$$\langle L(v) \rangle = \frac{\int_0^\infty L e^{-L/L_0} dL}{\int_0^\infty e^{-L/L_0} dL} = L_0(v) . \qquad (7)$$

At the same velocity a track of dip angle δ appears to have a mean gap length

$$\langle L'(v) \rangle = \frac{\int_{2a(\sec\delta - 1)}^\infty [(L+2a)\cos\delta - 2a]\, e^{-L/L_0} dL}{\int_0^\infty e^{-L/L_0}\, dL} \qquad (7A)$$

$$= L_0 \cos\delta \exp - \left[\frac{2a}{L_0} (\sec\delta - 1) \right].$$

The ratio of the observed fractional track transmission for a track at dip angle δ to that for a "flat" track of the same velocity is

$$T_\delta / T_0 = \langle L'(v)/L_0(v) \rangle = \exp \left[-\frac{2a}{L_0} (\sec\delta - 1) \right]. \qquad (8)$$

This is the expression for the dependence of the fractional transmission on dip angle. The parameter $\alpha = 2a/L_0$ is a function of the particle velocity, and was determined empirically by measuring the observed transmission of protons dipping at a known angle as a function of residual range. The dependence of α on residual range is shown in Fig. 10. By iteration the true transmission and the residual range of a steeply diving track are made known.

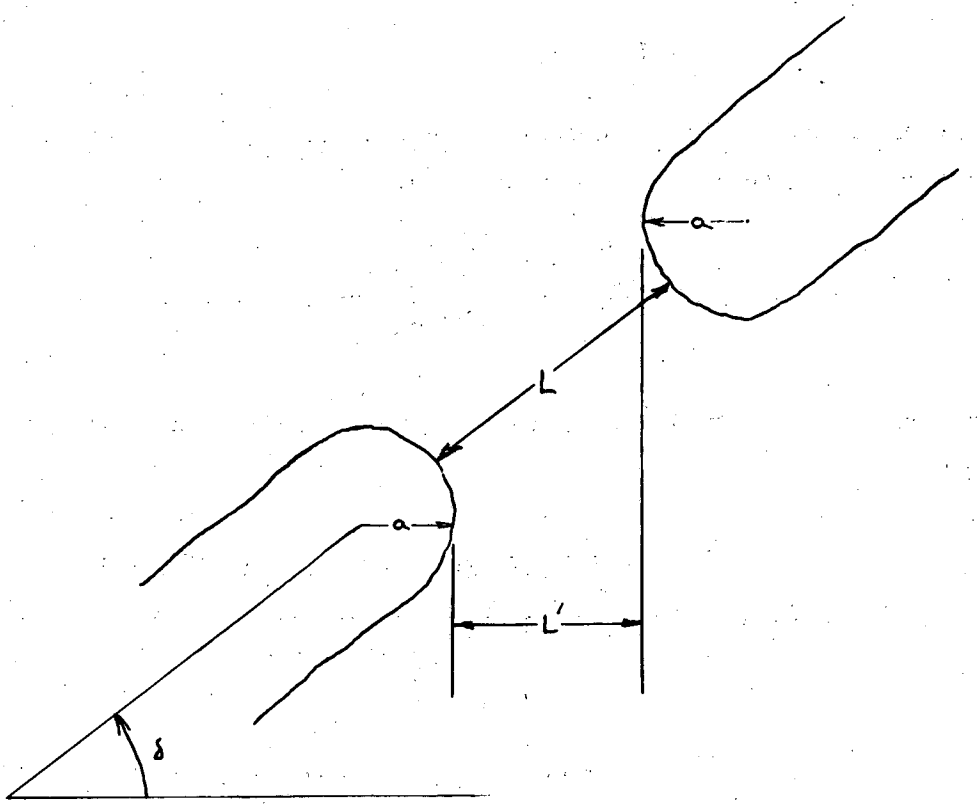

Fig. 9. Profile view of track-grain separation. L is the true separation, L' is the observed separation, a is the effective radius of the grain tips, and δ is the dip angle of the track with respect to the plane of the emulsion.

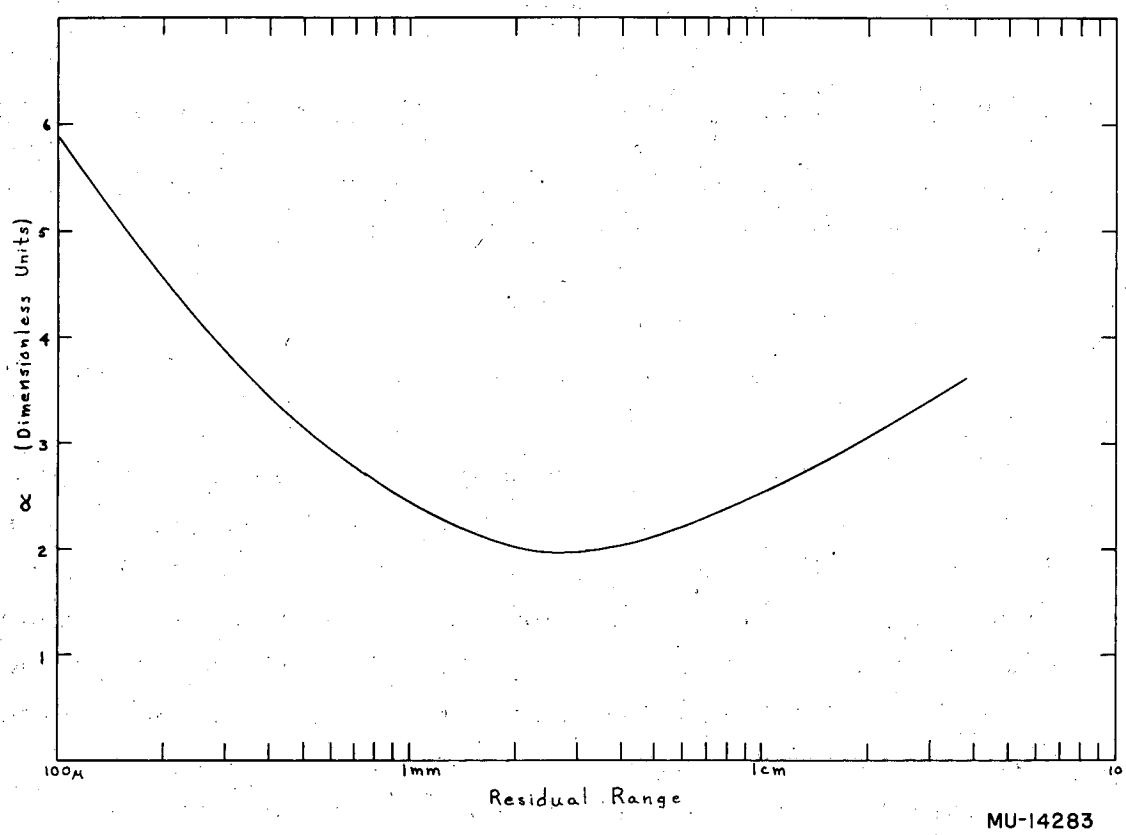

Fig. 10. The parameter α plotted versus the residual range of the track. It is derived empirically from the observation of stopping protons traveling at known dip angles.

The relative probability as a function of the decay rate is plotted by use of the 36 decays occurring in flight in the 2B stack. It is shown in Fig. 11. The observed most likely decay rate is $1.92 \pm 0.44 \times 10^{10}$ sec^{-1}, where the limits are for the values at half maximum. The limits reflect statistical uncertainties only. All calculations were programmed on an IBM type 650 computer. The effect of the experimental uncertainties in the fractional track transmission measurements will be considered next.

The Effect of Errors in Fractional Track Transmission Measurements

The most likely decay rate is that decay rate for which the derivative of Eq. (6) is zero. It is a solution of

$$1/r = \frac{\sum_{i=1}^{N} \left[t_i + \frac{T_i}{e^{rT_i} - 1} \right]}{N} , \qquad (9)$$

where N is the total number of events. The width of the curve in Fig. 11 defines the uncertainty in r from statistical sources. In addition there is an appreciable uncertainty in r due to the uncertainties in the fractional transmission measurements. These appear as uncertainties in the t_i and T_i. The effect is calculated as follows: Let r_0 be the most likely decay rate if there were no errors in the track transmission measurements. Let r be the most likely decay rate resulting from a set of deviations ΔF_i in the measured fractional track transmissions. Then, expanding in a Taylor's series, we obtain

$$r = r_0 + \sum_{i=1}^{N} \frac{\partial r_0}{\partial F_i} \Delta F_i + \frac{1}{2!} \sum_{i=1}^{N} \sum_{j=1}^{N} \frac{\partial^2 r_0}{\partial F_i \partial F_i} \Delta F_i \Delta F_j + \cdots . \qquad (10)$$

The ΔF_i are random variables distributed around zero. I shall assume their distribution to be nearly Gaussian. The mean value of $(r - r_0)$ is

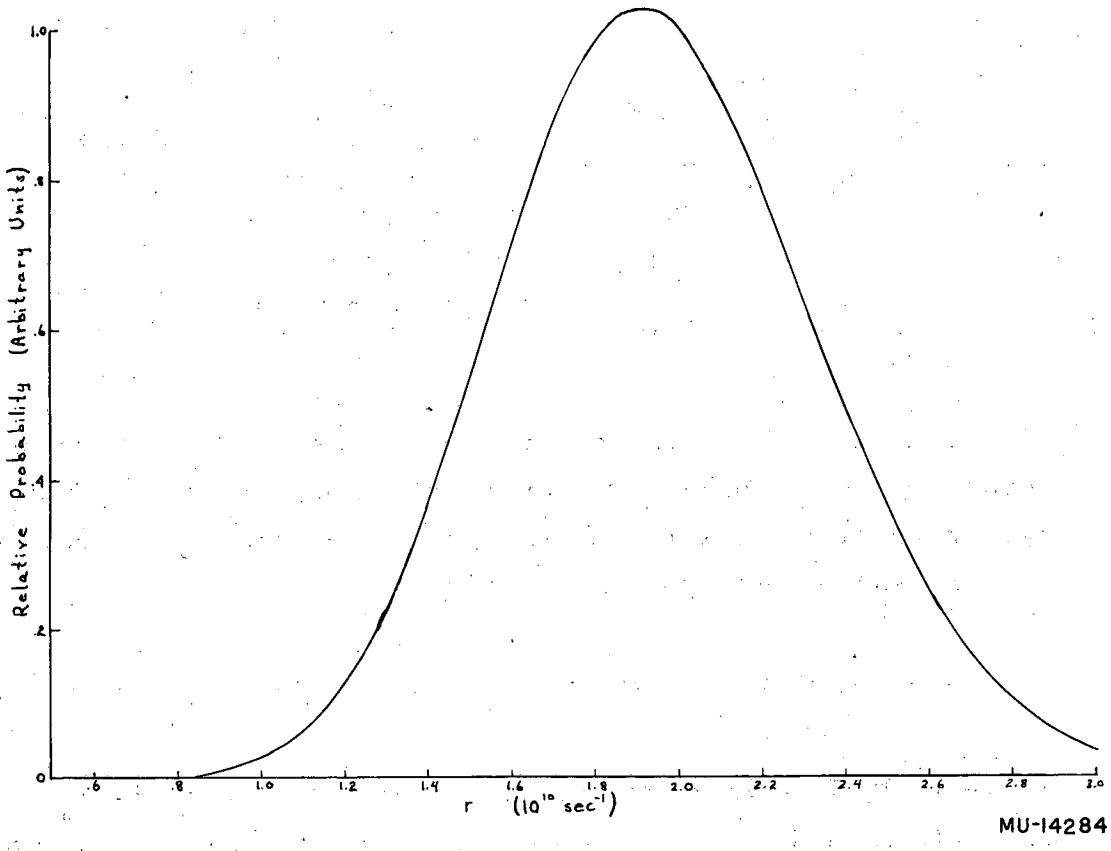

Fig. 11. The relative-likelihood function plotted versus r for all hyperons decaying in flight via the pion mode.

$$\left\langle r - r_0 \right\rangle = \frac{1}{2} \sum_{i=1}^{N} \frac{\partial^2 r_0}{\partial F_i^2} \left\langle \Delta F_i^2 \right\rangle + \cdots . \qquad (11)$$

The mean square value of $r - r_0$ is

$$\left\langle (r-r_0)^2 \right\rangle = \sum_{i=1}^{N} \left(\frac{\partial r_0}{\partial F_i} \right)^2 \left\langle \Delta F_i^2 \right\rangle + \frac{1}{4} \sum_{i=1}^{N} \left(\frac{\partial^2 r_0}{\partial F_i^2} \right)^2 \left\langle \Delta F_i^4 \right\rangle$$

$$+ \frac{1}{4} \sum_{\substack{i=1 \\ i \neq j}}^{N} \sum_{j=1}^{N} \left[\frac{\partial^2 r_0}{\partial F_i \, \partial F_j} \right]^2 \left\langle \Delta F_i^2 \right\rangle \left\langle \Delta F_j^2 \right\rangle + \qquad (12)$$

$$+ \frac{1}{4} \sum_{\substack{i=1 \\ i \neq j}}^{N} \sum_{j=1}^{N} \frac{\partial^2 r_0}{\partial F_i^2} \frac{\partial^2 r_0}{\partial F_j^2} \left\langle \Delta F_i^2 \right\rangle \left\langle \Delta F_j^2 \right\rangle + \cdots .$$

This is the expression for the uncertainty in r_0 due only to random errors in the F_i. In addition, the uncertainty in r_0 arising from systematic errors of the F_i (that is, any uncertainty in the comparison transmission-range curve) is given by

$$\left\langle r - r_0 \right\rangle = \pm \sum_{i=1}^{N} \frac{\partial r_0}{\partial F_i} F_i \left\langle \frac{\Delta F_i}{F_i} \right\rangle + \cdots + , \qquad (13)$$

where $\left\langle \Delta F_i / F_i \right\rangle$ is the systematic fractional error in the F_i. The calculations of the partial derivatives were carried out by a second IBM 650 program. The true most likely decay rate, r_0, calculated from Eq. (11), is

$$r_0 = 1.98 \times 10^{10} \text{ sec}^{-1}.$$

From Eq. (12) the mean square uncertainty in r_0 is

$$\left\langle (r - r_0)^2 \right\rangle = \left\langle \Delta r_0^2 \right\rangle = 0.041 \times 10^{20} \text{ sec}^{-2} .$$

I estimate that 5% is a fair assessment of the uncertainty in the transmission-range curve. Hence, according to Eq. (13) the systematic uncertainty is

$$\langle r - r_0 \rangle = \langle \Delta r_0 \rangle = \pm 0.600 \times 10^{10} \text{ sec}^{-1} .$$

If the effects of the statistical uncertainties and systematic and random errors are added quadratically, I obtain

$$r_0 = 1.98 \pm 0.77 \times 10^{10} \text{ sec}^{-1}$$

which corresponds to a mean life $\tau = 0.5 \pm 0.2 \times 10^{-10}$ sec. Recent data from the hydrogen bubble chamber experiments[5] indicate a Σ^+ hyperon decay rate of $1.4 \pm 0.2 \times 10^{10}$ sec^{-1}, and a Σ^- hyperon decay rate of 0.538×10^{10} sec^{-1}. One would expect a most likely decay rate to lie between these two values. Other observors,[19, 20] with less extensive analysis, conclude that a discrepancy exists.[20, 21] For the charge mixture I have just considered, the value appears to be larger than the upper limit, but in view of the large uncertainties due to measurement error, I do not believe there is any significance in it.

To test this last statement, the same procedure for determining the most likely decay rate was applied to those Σ^+ hyperons decaying in flight into protons. The 21 decays occurring in the 2B stack were used. The information about the hyperon energy at decay, as derived from the kinematics of the decay proton, were not used. Instead, track transmission measurements were made, just as in the charged-pion decay mode. The likelihood function is plotted in Fig. 12. The observed most likely decay rate is $0.520 \pm 0.470 \times 10^{10}$ sec^{-1}. The limits are at the half heights. From the IBM calculation of the partial derivatives, we have

$$\langle r - r_0 \rangle = \frac{1}{2} \sum_{i=1}^{N} \frac{\partial^2 r_0}{\partial F_i^2} = -0.383 \times 10^{10} \text{ sec}^{-1} .$$

The effect of the second derivatives is large, so that very possibly higher-order derivatives may be of importance. Roughly, we have

$$r_0 = 0.90 \times 10^{10} \text{ sec}^{-1} ,$$

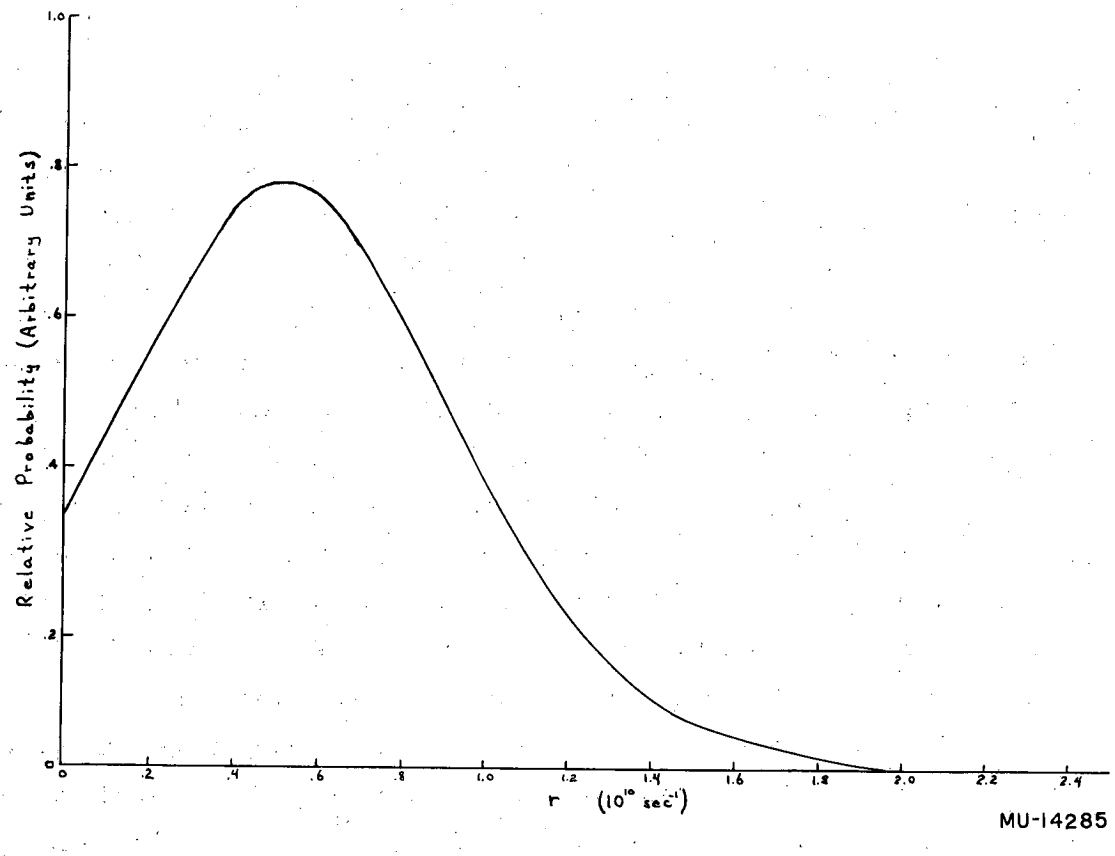

Fig. 12. The relative-likelihood function plotted versus r for those hyperons decaying in flight via the proton mode. The ordinate is arbitrary.

The mean square uncertainty in r_0 owing to random errors in measuring the F_i is given by Eq. (12). It is

$$\langle \Delta r_0^2 \rangle = 0.073 \times 10^{20} \text{ sec}^{-2} .$$

The uncertainty in r_0 arising from systematic errors in the track transmission-comparison curve is

$$\Delta r_0 = \Sigma \frac{\partial r_0}{\partial F_i} F_i \left\langle \frac{\Delta F_i}{F_i} \right\rangle = \pm 0.0236 \times 10^{10} \text{ sec}^{-1} .$$

Adding quadratically the statistical error and the systematic and random errors in measurement, one obtains

$$r_0 = 0.90 \pm 0.54 \times 10^{10} \text{ sec}^{-1} ,$$

corresponding to a mean life

$$\tau = 1.1 \pm 0.7 \times 10^{-10} \text{ sec.}$$

The Σ^+ and Σ^- Decay Rates Determined by the Pion Decay Mode

I shall now consider a second analysis, which will give more reliable information about the pion-decay mode of the Σ^+ hyperon, as well as some information about the Σ^--hyperon decay rate. For this analysis I include the decays at rest of the pion mode of the Σ^+ hyperon, and the interactions at rest of the Σ^- hyperons. If, as in the proton decay mode, we have available all events decaying at rest and decaying in flight, the likelihood function for r may be written

$$P(r) = \prod_{i=1}^{F} r e^{-rt_i} \prod_{j=1}^{R} e^{-rT_j} . \qquad (5)$$

If there are possibly two decay rates associated with each charge state, the likelihood function may be written

$$P(r^+, r^-) = \prod_{i=1}^{R^+} e^{-r^+T_i} \prod_{j=1}^{R^-} e^{-r^-T_j} \prod_{k=1}^{F} [P_k r^+ e^{-r^+tk} + (1-P_k) r^- e^{-r^-t_k}] \qquad (14)$$

where the first product is over those Σ^+ hyperons decaying at rest, the second product is over those Σ^- hyperons interacting at rest, and the third product is over those hyperons decaying in flight.

The P_k represent the probability that a specific hyperon decaying in flight is positively charged. In two cases the charge is known because the decay pion was followed. In the other cases the P_k may be estimated by examining the hyperon-production process. I have divided the charged hyperons of known charge into four phenomenological categories, those created with minimum-ionizing π-mesons only, those created with one heavily ionizing track, those created with two or more tracks, and those created with no other charged tracks. The fractions of Σ^+ hyperons created in these categories are denoted a^+_i, and the fractions of Σ^- hyperons are denoted a^-_i. Restricting our attention to the charged hyperons of uncertain charge decaying in flight, we find that the probability that a hyperon is positive and is associated with, say, a charged pion is fa^+_π, where f is the fraction of hyperons which are positive. Similarly the probability that the hyperon is negative and associated with a charged pion is $(1-f)\,a^-_\pi$. The value of f used assumes that the branching ratio between charged-pion and proton decay modes of the Σ^+ hyperon be unity. Experimentally I find 31 decaying at rest by the pion mode and 32 decaying at rest by the proton mode. Because there are 27 decays in flight via the proton mode, the assumption is, then, that there be about 27 decays in flight out of a total of 66 events; f is thus taken to be 0.409. The probability that a given hyperon that was created in one of the four categories listed above be positive may now be written

$$P^+_i = \frac{f\,a^+_i}{fa^+_i + (1-f)a^-_i} \quad . \tag{15}$$

The four probabilities that a hyperon be a Σ^+ are:

if created with a minimum-ionizing pion, 49.3%;

if created with a heavily ionizing track, 32.0%;

if created with no charged track, 15.8%;

if created with two or more tracks, 34.1% .

Whereas the Σ^+ hyperons decaying at rest through the pion mode are identifiable, Σ^- hyperons interacting at rest are not. Frequently hyperons interact at rest, leaving no hint that they are other than some common stable particle. We know this, for example, from observations of K^- mesons interacting with free protons in the emulsion, in which the hyperon apparently neither decays nor interacts at rest. Even Σ^- hyperons producing one-pronged stars are suspect. Often these appear to be no more than a proton elastically scattering at low energy. The only unambiguous cases are the hyperons that produce stars with two or more prongs. Gilbert, Violet, and White estimate that 35 ± 10% of all Σ^- hyperons interacting at rest produce two-pronged or larger stars.[13] Using their data, I can now estimate the total moderation time of all hyperons coming to rest by knowing only the total moderation time of those producing two-pronged or greater stars. Note that it is only the total moderation time that appears in the exponent of the second term in Eq. (14).

The most likely Σ^+-hyperon and Σ^--hyperon decay rates are solutions of the two minimal equations,

$$\frac{\partial \ell n\, P(r^+, r^-)}{\partial r^+} = 0$$

$$= -\sum_{i=1}^{R^+} T_i + \sum_{k=1}^{F} \frac{P_k e^{-r^+ t_k} (1 - r^+ t_k)}{P_k r^+ e^{-r^+ t_k} + (1 - P_k) r^- e^{-r^- t_k}} \qquad (16A)$$

$$\frac{\partial \ell n\, P(r^+, r^-)}{\partial r^-} = 0$$

$$= -\sum_{j=1}^{R^-} T_j + \sum_{k=1}^{F} \frac{(1 - P_k) e^{-r^- t_k} (1 - r^- t_k)}{P_k r^+ e^{-r^+ t_k} + (1 - P_k) r^- e^{-r^- t_k}} \qquad (16B)$$

The solutions, as calculated by the IBM 650 computer, are

$$r^+ = 1.65 \times 10^{10} \text{ sec}^{-1},$$
$$r^- = 0.589 \times 10^{10} \text{ sec}^{-1}.$$

In order to estimate the statistical uncertainty in the two decay rates I have plotted in Fig. 13 and 14 the likelihood function (a) for the Σ^+ decay, as a function of r at r^-_{max}, and (b) for the Σ^- decay as a function of r at r^+_{max}. For the Σ^--hyperon decay rate an additional uncertainty is incurred in the uncertainty of the fraction of Σ^- hyperons interacting to produce stars of two or more prongs (35 ± 10%). This error amounts to $\pm 0.206 \times 10^{10}$ sec^{-1} in the most likely Σ^--hyperon decay rate. This uncertainty is also reflected in the most likely Σ^+-hyperon decay rate. Its extent is $\pm 0.163 \times 10^{10}$ sec^{-1}. The following are the most likely decay rates and their uncertainties for charged hyperons decaying via the charged-pion mode:

$r^+_{max} = 1.650 \pm 0.38 \times 10^{10}$ sec^{-1}, corresponding to a mean life

$$\tau^+ = 0.61^{+0.18}_{-0.11} \times 10^{-10} \text{ sec},$$

$r^-_{max} = 0.59 \pm 0.24 \times 10^{10}$ sec^{-1}, which corresponds to a mean life

$$\tau^- = 1.7^{+1.1}_{-0.5} \times 10^{-10} \text{ sec}.$$

The combined maximum-likehood Σ^+-hyperon decay rate, as measured by both modes of decay, becomes

$$r^+ = 1.15 \pm 0.15 \times 10^{10} \text{ sec}^{-1}, \quad \text{or}$$

$$\tau^+ = 0.87^{+0.13}_{-0.10} \times 10^{-10} \text{ sec}.$$

The hydrogen-bubble-chamber estimate of the Σ^--hyperon lifetime is $1.6 \pm 0.2 \times 10^{-10}$ sec. The only previous emulsion estimate is of 2.3×10^{-10} sec, with a lower limit of 1.3×10^{-10} sec by Snow et al.[20]

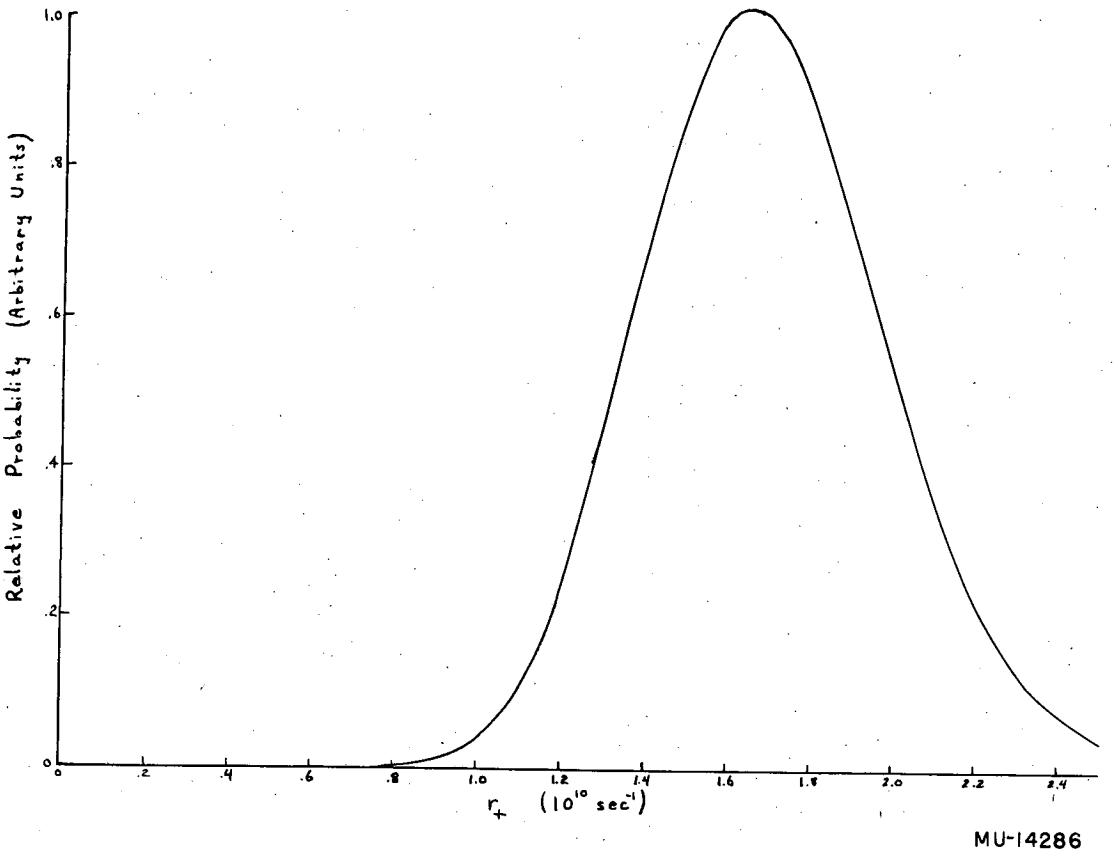

Fig. 13. The relative-likelihood function at r^-_{max} plotted versus r_+ for all hyperons not decaying through the proton mode. It pictures the statistical spread around the most likely Σ^+-hyperon decay rate. The ordinate is arbitrary.

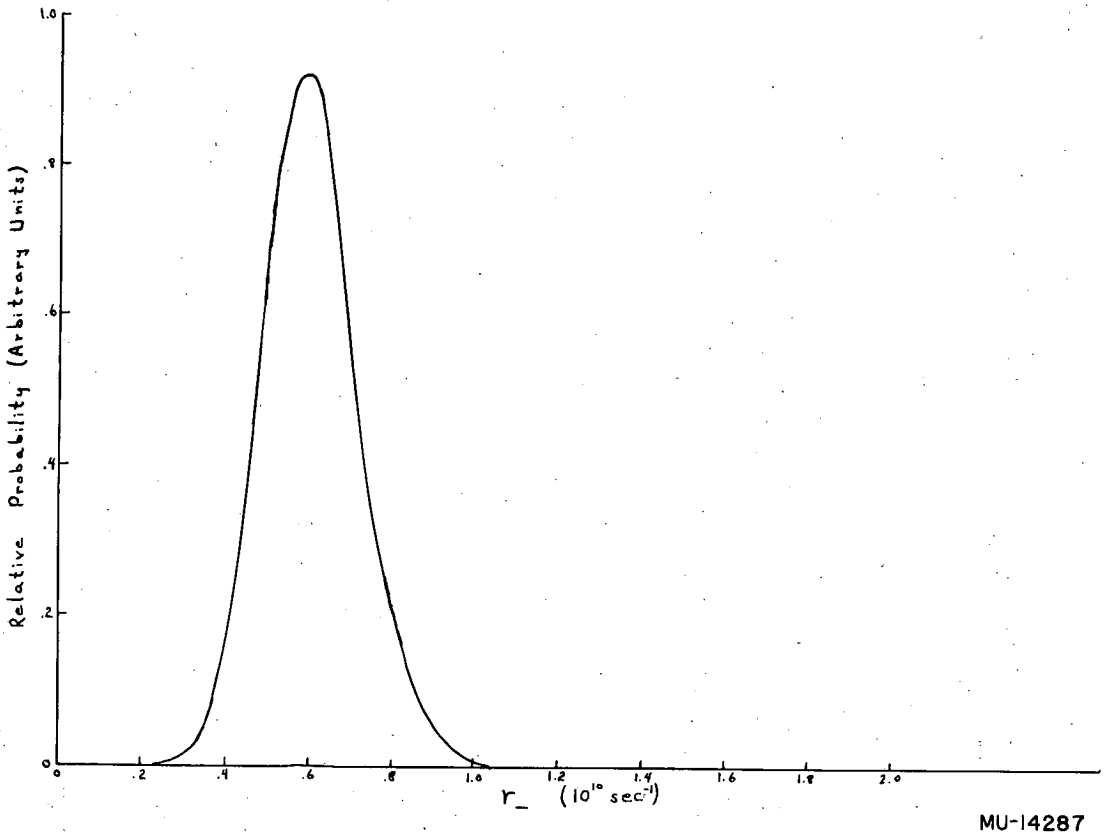

Fig. 14. The relative-likelihood function at r^+_{max} plotted versus r^- for all hyperons not decaying through the proton mode. It pictures the statistical spread around the most likely Σ^--hyperon decay rate. The ordinate is arbitrary.

THE HYPERON-DECAY ANGULAR DISTRIBUTION

The examination of the angular distribution of the decay-particle momentum vectors referred to some direction in space will provide some information about the spin, polarization, and parity-conservation characteristics of the hyperons. A natural reference direction is the normal to the plane defined by the hyperon and the pion created with it. There is tentative evidence (in work presented elsewhere) that an asymmetry exists.[23]

Another natural reference direction is the initial momentum vector of the hyperon. For those hyperons decaying at rest the angles between the hyperon-momentum vector and the decay-momentum vector are measured directly. For hyperons decaying in flight via the proton mode, the transformation of angles from laboratory system to center-of-mass system is quite accurate because the hyperon velocity at decay and the initial proton velocity are known quite well. The velocity at decay of those hyperons decaying through the pion mode is known less well. However, the center-of-mass angle may still be calculated accurately because the pion velocity is much greater than the hyperon velocity and thus the difference between laboratory and center-of-mass angles is small.

The angular distributions of the neutral pions coming from hyperons decaying through the proton mode are displayed in Figs. 15 and 16. Figure 16 is the same distribution folded about 90° as a means of showing even powers of cosine θ. The angular distribution of the charged pions coming from hyperons decaying through the pion mode is displayed in Fig. 17. Similarly Fig. 18 shows the distribution folded about 90°. The two distributions appear to be isotropic. The pion-mode distribution differs from isotropy by about one standard deviation. This is to be expected in about one out of every three distributions. No strong conclucions can be drawn, although it seems more likely, on the basis of this experiment, that the hyperon has spin $1/2\hbar$. A spin-$1/2\hbar$ particle will always decay isotropically, provided parity is conserved, regardless of the polarization. If parity is not conserved, and the hyperon is

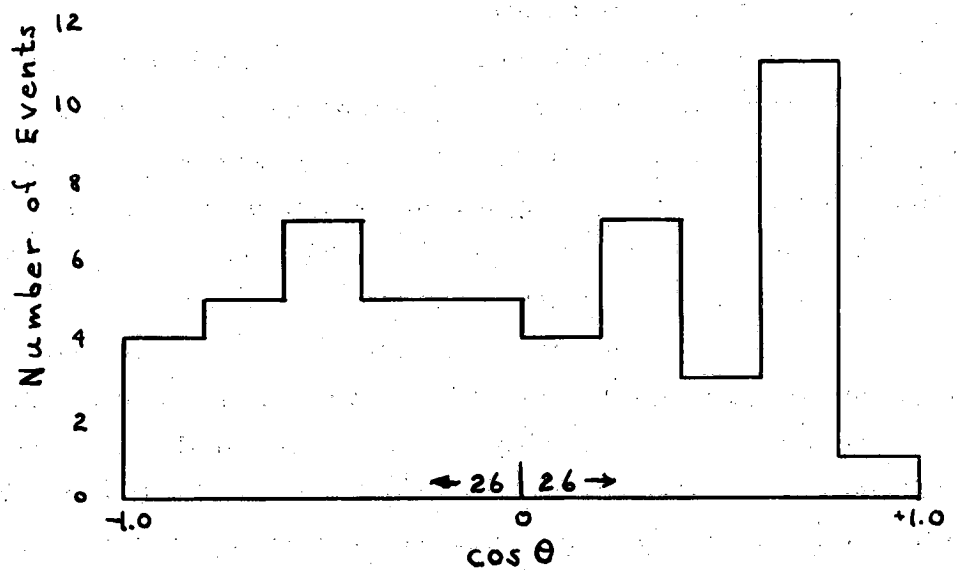

Fig. 15. The angular distribution of hyperons decaying into protons. The angle θ is that between the neutral pion and the hyperon in the center-of-mass system.

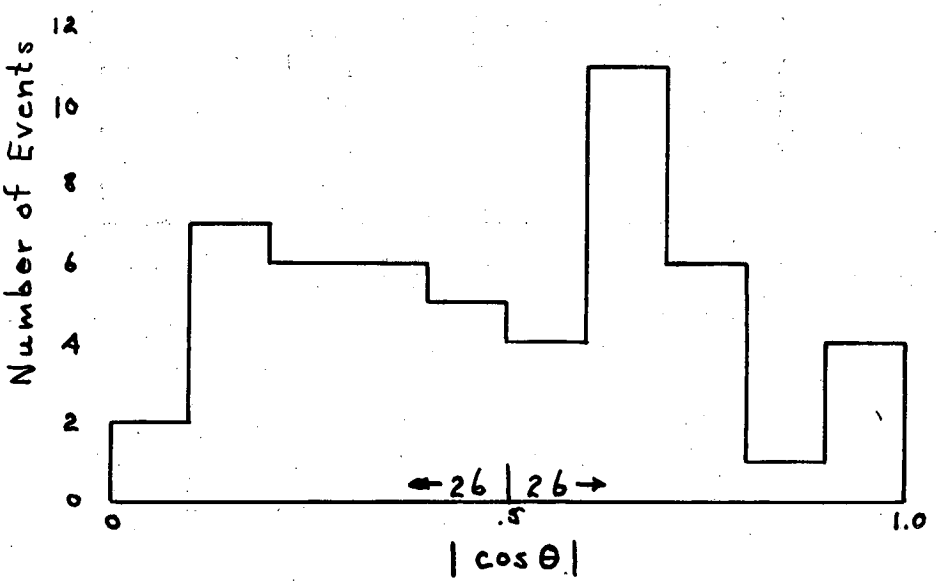

MU-14289

Fig. 16. The angular distribution of hyperons decaying into protons, folded about 90°. There is no apparent dependence on cosine θ.

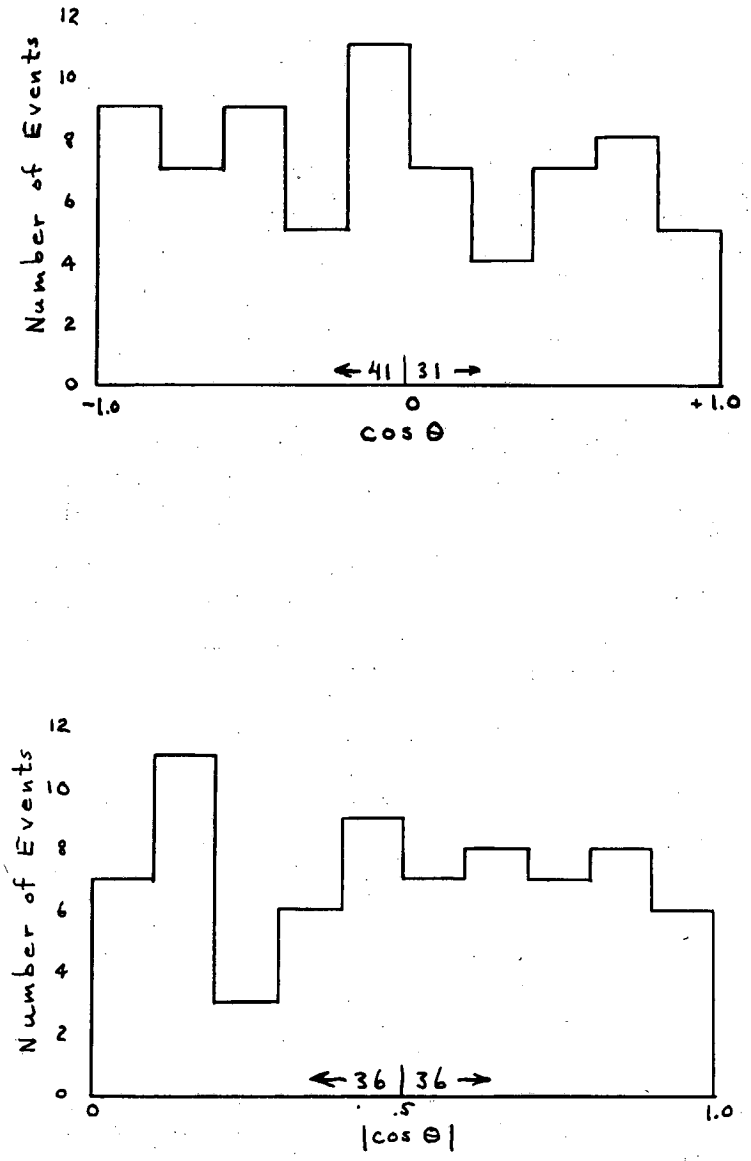

Fig. 17 and 18. The angular distributions of hyperons decaying into the pion mode. The angle θ is that between the charged pion and the hyperon.

polarized, a $\cos\theta$ term will appear. I conclude that there is no evidence for parity nonconservation here.

ACKNOWLEDGMENTS

I would like to thank Dr. Walter H. Barkas for suggesting and directing this research. I also would like to thank Dr. Fred W. Inman for helping to program the first calculation on the IBM 650 computer, and Dr. F. C. Gilbert for making available to me copies of curves relating the center-of-mass and laboratory angles between the hyperons and their decay products.

This work was done under the auspices of the U. S. Atomic Energy Commission.

REFERENCES

1. York, Leighton, and Bjornerud, Phys. Rev. 90, 167 (1953).
2. Bonnetti, Levi-Setti, Panetti, and Tomasini, Nuovo Cimento 10, 345 (1953).
3. J. Hornbostel and E. O. Salant, Phys. Rev. 98, 218 (1955).
4. M. Gell-Mann and A. Pais, Proceedings of the Glasgow Conference, 1954.
5. L. W. Alvarez, H. Bradner, P. Falk-Vairant, D. Gow, A. H. Rosenfeld, F. Solmitz, and R. Tripp, Interactions of K^- Mesons in Hydrogen, UCRL-3775, July 1957.
6. J. Hornbostel and E. O. Salant, Phys. Rev. 93, 902 (1954).
7. W. H. Barkas, W. F. Dudziak, P. C. Giles, H. H. Heckman, F. W. Inman, C. J. Mason, N. A. Nickols, and F. M. Smith, Results from an Enriched Negative K-Meson Beam, UCRL-3627, Dec. 1956.
8. W. W. Chupp, G. Goldhaber, S. Goldhaber, and F. H. Webb; Phys. Rev. 100, 959A (1955).
9. C. E. Violet, F. C. Gilbert, and R. S. White; Phys. Rev. 100 1803A (1955).
10. D. M. Haskin, T. Bowen, and M. Schein, Phys. Rev. 103, 1512 (1956).
11. W. H. Barkas, P. H. Barrett, P. Cuer, H. H. Heckman, F. M. Smith, and H. K. Ticho; The Range-Energy Relation in Emulsion. Part I: Range Measurements, UCRL-3768, April 1957
12. W. H. Barkas, The Range-Energy Relation in Emulsion, Part 2. The Theoretical Range, UCRL-3769, April 1957.
13. F. C. Gilbert, C. E. Violet, and R. S. White, Negative K-Particle Captures by Bound and Free Protons in Emulsion, UCRL-4814, Feb. 1957.
14. Fry, Schneps, Snow, Swami, and Wold, Phys. Rev. 104, 270 (1956).

15. Chupp, Goldhaber, Goldhaber, and Webb, in Physics Division Quarterly Report, UCRL-3593, Nov. 1956.
16. J. Steinberger, in Proceedings of the Sixth Annual Rochester Conference on High-Energy Physics, 1956 (Interscience, New York).
17. S. Goldhaber, ibid.
18. S. C. Freden and H. K. Ticho, Phys. Rev. 105, 1121 (1957).
19. M. S. Bartlett, Phil. Mag. 44, 249 (1953).
20. Snow, Fry, Schneps, Swami, and Wold, Bull. Am. Phys. Soc. 2, 19 (1957).
21. Seeman, Glasser, and Snow, Bull. Am. Phys. Soc. 2, 223 (1957).
22. C. O'Ceallaigh, Proc. Roy. Soc. January, 1954.
23. Alles, Biswas, Ceccarelli, Crussard, Barkas, Giles, Heckman, Inman, and Smith, Parity Nonconservation in Hyperon Decays, UCRL-3895 (Abstract), Aug. 1957